Electronic states of Si(100) reconstructed surfaces

Zizhong Zhu,* Nobuyuki Shima, and Masaru Tsukada
Department of Physics, Faculty of Science, University of Tokyo, Hongo 7-3-1, Bunkyo-ku, Tokyo 113, Japan
(Received 27 April 1989; revised manuscript received 28 August 1989)

The detailed electronic structures and geometries of Si(100) reconstructed surfaces are investigated by a self-consistent calculation with a norm-conserving nonlocal pseudopotential. We concentrate on the dimer model and on (2×1), $p(2\times2)$, and $c(4\times2)$ reconstructions which are simultaneously detected by recent scanning-tunneling-microscopy measurements. The optimized geometries of asymmetric (2×1) and $c(4\times2)$ systems are reached by minimizing the total energy. Present study shows that the $c(4\times2)$ system is the most favorable one at absolute zero temperature; moreover, the $p(2\times2)$ system can also be favored because the total-energy difference between $c(4\times2)$ and $p(2\times2)$ systems is relatively small. Both of them are much more stable than (2×1) buckled structure. The surface electronic structures of $p(2\times2)$ and $c(4\times2)$ systems are analyzed and understood based on the electronic structure of (2×1) asymmetric-dimer model. Both the surface band structures and optimized geometries of the present calculation are in reasonably good agreement with experiments.

I. INTRODUCTION

There has been considerable theoretical and experimental interest in the electronic and geometric structure of semiconductor surfaces, especially of the silicon surface. The silicon (100) surface has been one of the simplest yet still controversial systems, which has been investigated for about 30 years since Schlier and Farnsworth[1] first provided evidence for top-layer atoms pairing leading to a (2×1) reconstruction. Many reconstruction patterns have been observed on this surface since then, for example, (2×1),[2-4] $p(2\times2)$, $c(4\times2)$,[5-9] $c(4\times4)$,[10] and also $(2\times n)$ $(6\leq n\leq10)$.[11,12] Some of them are detected only within relatively narrow temperature regions. Many different structural models, which can be grouped into three classes: (a) dimer models,[13-21] (b) conjugated chain models,[22-24] and (c) vacancy models,[1,8,25] have also been conjectured. Of the structural models proposed for this surface, the dimer model (symmetric or asymmetric) is most widely supported both by experiments and theoretical calculations. Recently, scanning-tunneling-microscopy (STM) measurement[20,21] at room temperature on the Si(100) surface showed only buckled or nonbuckled dimerlike structure with random vacancies. Another result from this experiment is the presence of (2×1), $p(2\times2)$, and $c(4\times2)$ domains simultaneously on the same surface. Although this probably depends on the preparation method of the clean surface and on remaining surface impurities, there is little doubt that such a feature is presented on any experimentally used surface. The coexistence of different reconstructions together with vacancies on the same surface complicates the interpretation of some of the experimental results which may average over a large surface area. At such a case, theoretical studies on a particular reconstructed surface can be helpful and necessary for understanding the properties of a real surface.

Previous theoretical studies on the dimer model have all contributed significantly to our understanding of this reconstructed surface. On the basis of the Keating strain-energy minimization calculation, Appelbaum and Hamann[13] showed that the surface dimerization is accompanied by substantial subsurface distortions extending 4–5 atomic layers into the bulk. By using a tight-binding calculation, Chadi[14] suggested that the surface energy could be lowered further by allowing the dimers to buckle out of the surface plane. Later, the minimum-energy atomic geometry is presented by computing the Hellmann-Feynman forces and the total energies with the local pseudopotential method.[16] Other buckled dimer models have also been presented.[19] Ihm *et al.*[6] pointed out that the (2×1) structure is not the ground state of the Si(100) surface and higher-order reconstructions should occur on this surface at low temperature. They also predicted a transition temperature at about 250 K for the disappearance of higher-order spots. Recent experiments have shown clear $c(4\times2)$ low-energy electron diffraction (LEED) patterns at lower temperature.[26] However, for all these systems, the available results are not considered enough to regard the problem as completely solved; for example, neither the detailed electronic structures of higher-order reconstructions nor the reason for the lower energy of the $c(4\times2)$ reconstruction at low temperature are clear. Also, there are no conclusive determinations of the atomic arrangement including deep relaxations for higher-order reconstructions.

In this work, the norm-conserving nonlocal-pseudopotential approach is used to investigate detailed electronic and geometric structures of clean Si(100) surfaces. We concentrate on the dimer model and on (2×1), $p(2\times2)$, and $c(4\times2)$ reconstructions which are simultaneously detected by STM measurement. The optimized geometries of asymmetric (2×1) and $c(4\times2)$ systems are reached by minimizing the total energy with the guide of Hellmann-Feynman forces. Present study shows that the $c(4\times2)$ system is the most favorable one at absolute zero temperature; moreover, the $p(2\times2)$ system could also be favored because the total energy difference

 ©1989 The American Physical Society

between $c(4\times2)$ and $p(2\times2)$ systems is relatively small. Both of them are much more stable than the (2×1) asymmetric dimer model. The surface electronic structures of $p(2\times2)$ and $c(4\times2)$ systems are analyzed and understood based on the electronic structure of the (2×1) buckled dimer model. In the next section, the calculational procedure is described. Section III is dedicated to the discussions of the electronic structures of several Si(100) reconstructed surfaces and to a comparison of results with experiments. Their total energies and the ground state of the Si(100) surface are presented in Sec. IV. In Sec. V, optimized geometries of asymmetric (2×1) and $c(4\times2)$ surfaces and discussions concerning them are given. A summary of the results is shown in the last section.

II. CALCULATION METHOD

In the present work, we use a norm-conserving pseudopotential approach within the Hohenberg-Kohn-Sham local-density-functional formalism. This approach has been demonstrated to achieve accurate results in describing the electronic properties and a variety of structural properties for both extended and localized systems.[27] The valence electrons play a dominant role even in the determination of structural properties of materials; therefore, the computation of core states can be reasonably eliminated.

The ionic pseudopotential representing the effective core-valence electron interactions used in this study is the norm-conserving nonlocal one. Because of the large unit cell, the soft pseudopotential, which is constructed by the same procedure as in Ref. 28, is used in this work. The analytical form of this potential is given by Eqs. (2.1)–(2.3):[28]

$$\hat{V}_l^{\text{ion}}=\hat{V}_{\text{core}}(r)+\Delta\hat{V}_l^{\text{ion}}\ , \tag{2.1}$$

$$\hat{V}_{\text{core}}(r)=-\frac{Zv}{r}\sum_{i=1}^{2}C_i^{\text{core}}\text{erf}[(\alpha_i^{\text{core}})^{1/2}r]\ , \tag{2.2}$$

$$\Delta\hat{V}_l^{\text{ion}}(r)=\sum_{i=1}^{3}(A_i+r^2A_{i+3})e^{-\alpha_i r^2}\ . \tag{2.3}$$

TABLE II. Comparison of the calculated and measured static properties of silicon.

	Lattice constant (Å)	Cohesive energy (eV)	Bulk modulus (Mbar)
Calculation	5.424	4.465	0.948
Experiment	5.429	4.63	0.99
Difference	−0.1%	−3.6%	−4.0%

The values of potential parameters which come from Ohno[29] are given in Table I. The effect of the soft core of this potential is checked by its application to the silicon bulk properties. The comparison of calculated and measured static properties[27] is given in Table II. The exchange-correlation interaction is approximated by the $X\alpha$ potential with $\alpha=0.7$. The cohesive energy was obtained including the spin-polarized correction energy,[27] which is -0.075 Ry/atom within the $X\alpha$ potential approximation. The agreement of the calculated lattice constant, cohesive energy, and bulk modulus with experiment is satisfactory. Thus this potential may be applied to a system where Si—Si bond lengths are not so much different from that of bulk Si. In the following we suppose that this potential can be applied to our systems.

To facilitate the standard pseudopotential method, the repeated slab model is used to simulate the actual surface. The unit supercell consists of ten layers of silicon plus a vacuum region equivalent to about five layers of Si in thickness. A plane-wave basis set is employed for the expansion of the wave functions. The exchange-correlation interaction is approximated by the $X\alpha$ potential with $\alpha=0.7$. The plane waves up to 2.4 Ry in kinetic energy are included in the basis set. The cutoff is increased to 3.0 Ry in the test calculation of the (2×1) system, but there is no significant change of the band structures of the system. Hellmann-Feynman forces are also calculated and the absolute maximum difference between the corresponding forces for the two cutoffs is the order of 10^{-3}

TABLE I. The values of pseudopotential parameters.

	$Z_v=4.0$ $c_1^{\text{core}}=1.6054$ $c_2^{\text{core}}=-0.6054$		$\alpha_1^{\text{core}}=2.16$ $\alpha_2^{\text{core}}=0.86$
	$l=0$	$l=1$	$l=2$
A_1	−106.508 681 483 5	−127.753 717 108 8	−9853.758 600 006 9
A_2	−713.158 210 338 4	−180.973 295 552 7	2433.525 959 882 3
A_3	826.097 399 481 2	313.699 199 258 6	7422.255 383 417 5
A_4	13.151 447 978 4	15.003 439 488 4	882.625 296 807 8
A_5	335.744 985 971 8	152.934 278 507 3	4103.286 930 091 7
A_6	229.102 722 325 7	87.676 513 587 9	1323.568 741 763 4
α_1	1.10	0.90	1.15
α_2	1.80	1.40	1.45
α_3	2.40	2.00	1.90

Ry/a.u., which is small enough to get the same optimized geometries. Therefore, the cutoff of 2.4 Ry is used for present calculations of all systems, which leads to 1600–1700 plane waves for $p(2\times2)$ and $c(4\times2)$ systems.

Total energy and Hellmann-Feynman forces are computed after the self-consistent calculation. The method is standard and details of it are to be found elsewhere.[30] The optimized geometry is obtained by minimizing the total energy. For the optimizing process, the next step geometry is determined by using total energy and its derivatives of atomic positions (i.e., Hellmann-Feynman forces acting on each atoms) as a guide. The procedure is repeated until the forces on every atom of the unit cell become sufficiently small: for the buckled (2×1) system, all force is less than 3.0×10^{-3} Ry/a.u., and for the $c(4\times2)$ system it is less than 4.5×10^{-3} Ry/a.u. More precise optimization has not been performed, because the results do not change significantly in spite of huge computer time needed for such a large system, e.g., with 40 atoms and a large vacuum region per unit cell.

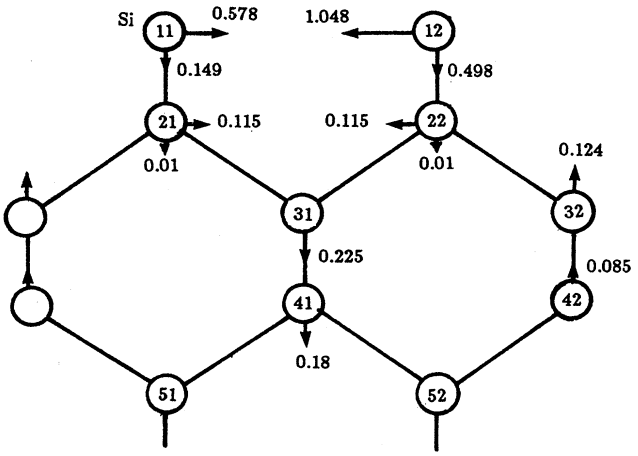

FIG. 2. Geometry of a single dimer used for comparing calculations of (2×1), $p(2\times2)$, and $c(4\times2)$ systems; units are Å.

III. ELECTRONIC STRUCTURES OF Si(100) (2×1), $p(2\times2)$, AND $c(4\times2)$ SURFACES

Figure 1 shows the top view of (2×1), $p(2\times2)$, and $c(4\times2)$ systems and their unit cells. All three systems include asymmetric dimers, identical in character, differing only in the way of dimer ordering on the surface. In order to see which way of dimer ordering is the most energy favorable one and to have a clear comparison of their electronic structures, in this and the next section all geometries for asymmetric (2×1), $p(2\times2)$, and $c(4\times2)$ surfaces used in the calculation have the exact same subsurface atomic positions (atoms 21, 22, 31, 32, 41, 42, 51, and 52 in Fig. 2) if there is no special statement of the geometry. The geometry used for a single dimer is shown in Fig. 2, which is obtained by a modification of the optimized geometry provided by Yin and Cohen,[16] in order to have the same subsurface geometries for all the (2×1), $p(2\times2)$, and $c(4\times2)$ systems.

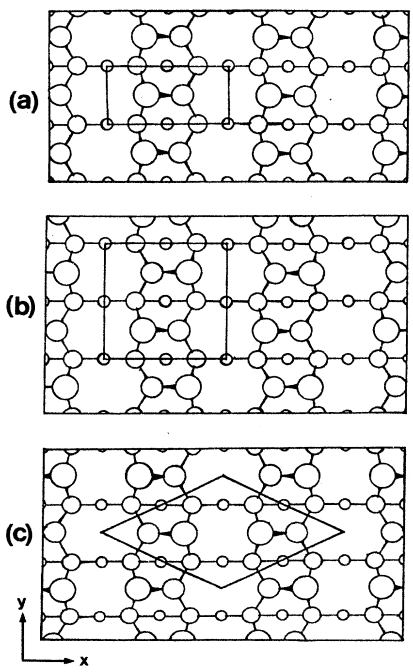

FIG. 1. Top view and unit cell of (2×1), $p(2\times2)$, and $c(4\times2)$ systems of the dimer model.

A. Symmetric and asymmetric dimer model of (2×1) reconstruction

In order to make a comparison with previous calculations and to check the present one, we have first performed the calculation for the symmetric dimer (2×1) model. The geometry used is Levine's model[31] in which only the first layer atoms of the surface are reconstructed to form a symmetric dimer with the dimer bond length equal to the bulk one. The calculated surface band structure and charge-density plots are shown in Figs. 3 and 4 together with those of the asymmetric (2×1) case. The two surface bands of symmetric dimer model are shown by dashed lines in the Fig. 3. Present calculation shows consistent results with the previous calculations.[14,15] For example, two parallel overlapping surface bands show the metallic character of the surface; the theoretical bandwidth of the occupied surface band (1.23 eV) is wider than the experimental ones [0.65 eV (Ref. 32) and 0.80 eV (Ref. 33)]. More detailed comparison of the (2×1) dispersion will be presented later.

For the (2×1) asymmetric dimer case, the most striking feature in this calculation is that the asymmetric dimer model results in a metallic surface, although two surface bands are repelled from each other to a large extent compared with the symmetric dimer case. This feature is in disagreement with photoemission data[32,33] and earlier theoretical calculations by Chadi[14] and Ihm and Cohen.[15]

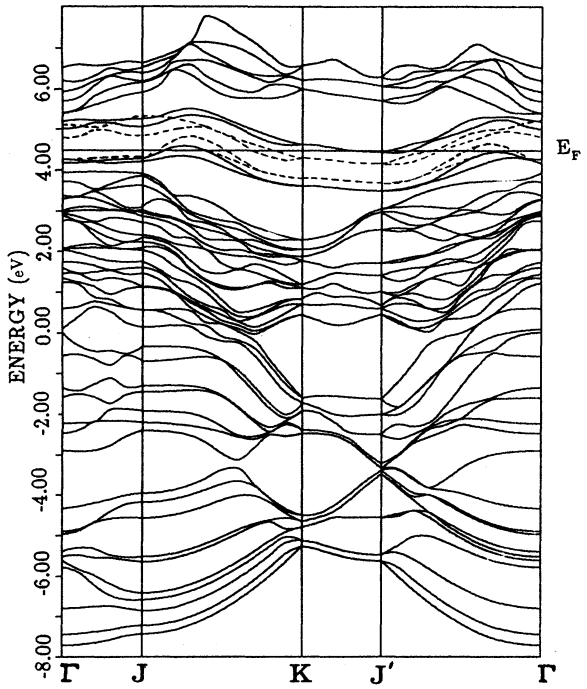

FIG. 3. Surface band structures of (2×1) symmetric- and asymmetric-dimer models. Bands of the asymmetric-dimer model are represented by solid lines. In the main gap region, the surface bands for the symmetric-dimer model are given by dashed lines.

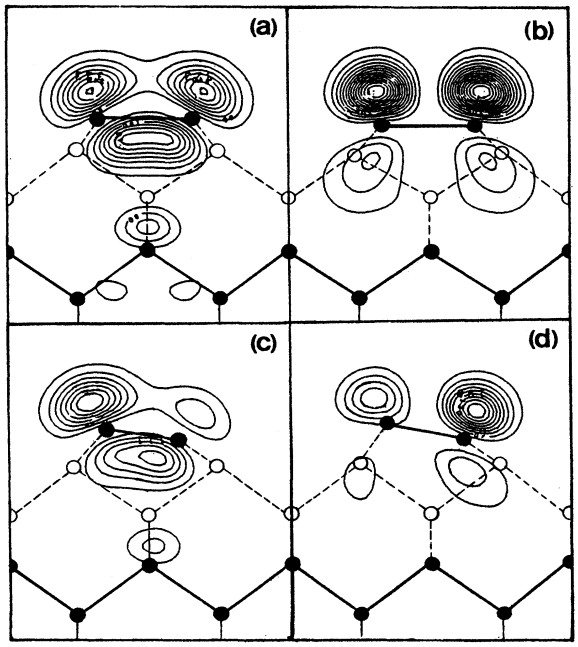

FIG. 4. Contour plots of square of wave functions at the J' point in (2×1) BZ. (a) Surface bonding and (b) antibonding states for symmetric dimer model. (c) Surface bonding and (d) antibonding states for the asymmetric dimer model. The plots are in a (110) plane cutting the surface at a right angle. The solid circles represent the Si atoms lying on the plane, and the solid lines between them represent the hypothetical covalent bonds. Si atoms not on the plane are denoted by open circles.

They both got the semiconducting feature with gaps of 0.6 eV and about 0.1 eV, respectively. However, a recent study by Kruger and Pollman[34] using the Green's function scattering formalism also obtained metallic surface bands. Moreover, Pandey's calculation[35] also showed a metallic surface for the buckling dimer model using the self-consistent pseudopotential method. The main feature of those calculations is consistent with the present one. The reason for the different results is discussed below.

Chadi's calculation was done using the tight-binding method, which usually cannot predict the energy gap quantitatively. As for Ihm and Cohen's calculation, the pseudopotential used is the local one together with a relatively small number of basis sets. We have performed the same local-pseudopotential calculation by using the same geometry and also by the $X\alpha$ exchange-correlation potential. It showed that the semiconducting surface was obtained only at low cutoff with $\alpha=0.8$. Increasing the cutoff or decreasing the α value to 0.7 will cause the band gap to vanish. As for the influence of the thickness of the slab used on the surface band structures, we have checked the results for the (2×1) system by using a slab with 12 silicon layers. It shows no substantial change of the conducting feature of this surface, see Fig. 5.

In the experiments, a semiconducting surface for the (2×1) structure is observed.[32,33] The discrepancy between theoretical calculations and experimental measurements may be due to several reasons. The present calculations are based on the local-density-functional approximation. It has been widely shown in the past that such an approximation greatly underestimates the band gap.[36] Another possibility for the difference is that the sample surface used in the experiments at finite temperature is

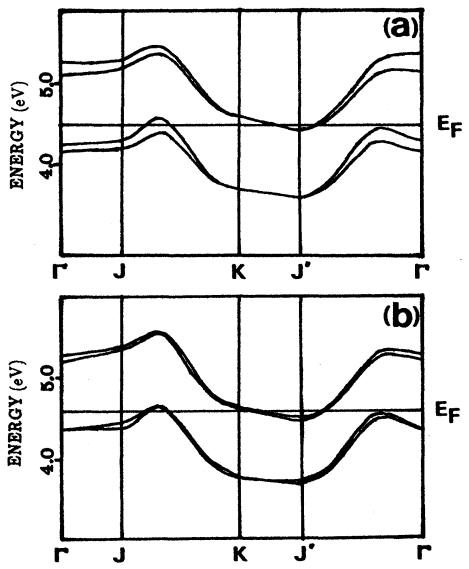

FIG. 5. Surface bands of asymmetric (2×1). (a) Using a slab of 10 silicon layers; (b) using a slab of 12 silicon layers.

not a perfectly buckled (2×1) structure, but with the random mixture of the microdomains of $c(4\times2)$ or $p(2\times2)$ structures. It remains unknown whether the perfect (2×1) surface of asymmetric dimers is metallic or semiconducting.

B. $p(2\times2)$ and $c(4\times2)$ reconstructions

The electronic feature of the $p(2\times2)$ surface is metallic, like that of the (2×1) asymmetric dimer one, as shown in Fig. 6(a). However, that of the $c(4\times2)$ surface is semiconducting with a very small indirect gap (~0.01 eV) between the π band state at point J and π^* at Y as shown in Fig. 7(a). These results can be understood on the electronic structures of the asymmetric (2×1) model, because $p(2\times2)$ and $c(4\times2)$ surfaces are both obtained by arraying the (2×1) buckled dimers on the surface, differing only in the way of ordering of dimers.

Figure 6(b) shows the surface band structure obtained directly from the folding of the energy bands of the asymmetric (2×1) surface in the Brillouin zone (BZ) of $p(2\times2)$ symmetry. Comparing the real bands of the $p(2\times2)$ surface with the folded ones of the (2×1) surface, slight lowering and raising of the occupied and unoccupied surface bands are observed around the Fermi level for the real $p(2\times2)$ calculation, but otherwise band structures are substantially the same. The result implies the weakness of influences on the electronic behavior of the system when neighboring dimers of the same dimer row buckled in different directions. From the calculated Fermi surfaces of the $p(2\times2)$ system and the folded one from the (2×1) surface, as shown in Figs. 10(d) and 10(b), it shows that "electron-hole" interactions are weak when the system changes from (2×1) symmetry to $p(2\times2)$ symmetry, and the metallic character of the surface is not changed. If we look at the wave functions at the Γ point for the bonding and antibonding surface states of the real $p(2\times2)$ structure, they show nearly the same character as those in the (2×1) case at the J' point,

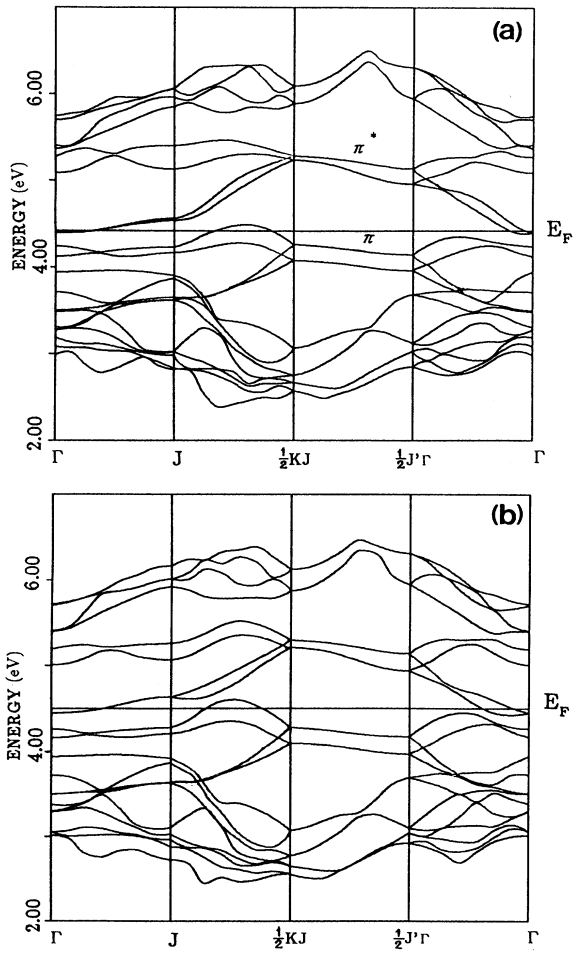

FIG. 6. Band structure of $p(2\times2)$ with the geometry of Fig. 2. (b) Band structure gained from folding (2×1) bands for $p(2\times2)$ symmetry.

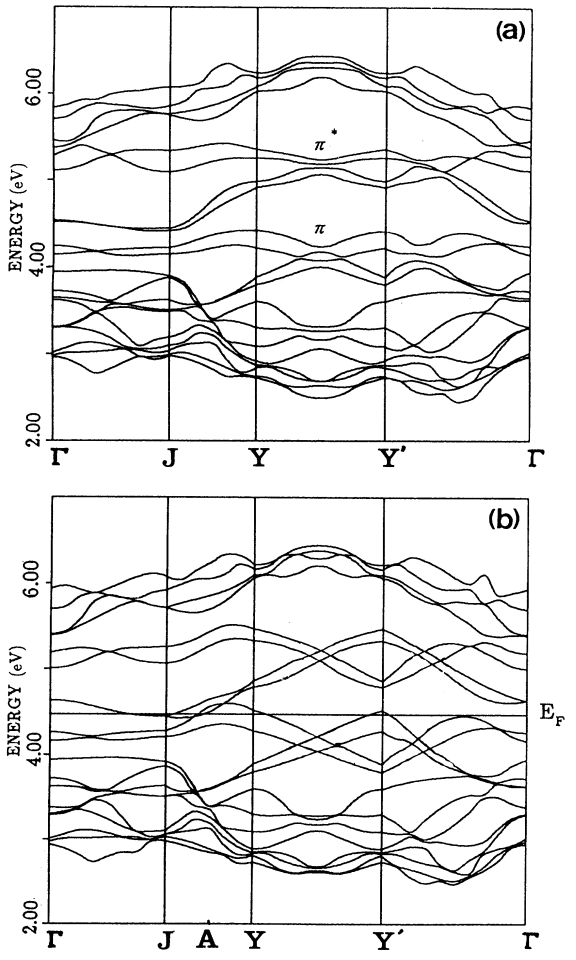

FIG. 7. Band structure of $c(4\times2)$ with the geometry of Fig. 2. (b) Band structure gained from folding (2×1) bands for $c(4\times2)$ symmetry.

which is folded to the Γ point at the $p(2\times2)$ BZ [see Figs. 4(c) and 4(d)]. This implies that the mixing is weak between bonding and antibonding states of surface dangling bonds when the ordering of surface dimers changes from the (2×1) structure to the $p(2\times2)$ one.

In contrast with the case of $p(2\times2)$, the $c(4\times2)$ surface becomes semiconducting while the surface bands folded from the (2×1) surface are clearly metallic, as seen in Figs. 7(a) and 7(b). The change of the conducting feature from metallic to semiconducting can be understood similarly from the analysis of wave function and the Fermi surface. Figures 8(c) and 8(d) show the square of the wave functions of the $c(4\times2)$ system and Figs. 8(a) and 8(b) show the corresponding quantity for the (2×1) structure. Shown are both the surface bonding (π) and antibonding (π^*) states at a point A along the $J-Y$ line in the $c(4\times2)$ BZ, where the Fermi surfaces of the folded (2×1) band have a region of overlapping [see Fig. 10(c)]. Comparing the wave functions for the two cases, it is shown that the bonding and antibonding states of the real $c(4\times2)$ system have the character of strong mixings of the bonding and antibonding states of surface dangling bonds of the (2×1) surface. It means that the hybridization between Bloch sums contributed from the dangling bonds on the up-buckled dimer atoms and that from the down-buckled dimer atoms is reduced around the A point in the $c(4\times2)$ case. This reduction leads the wave function at the A point of the $c(4\times2)$ BZ to have the same feature as that shown in Figs. 8(c) and 8(d).

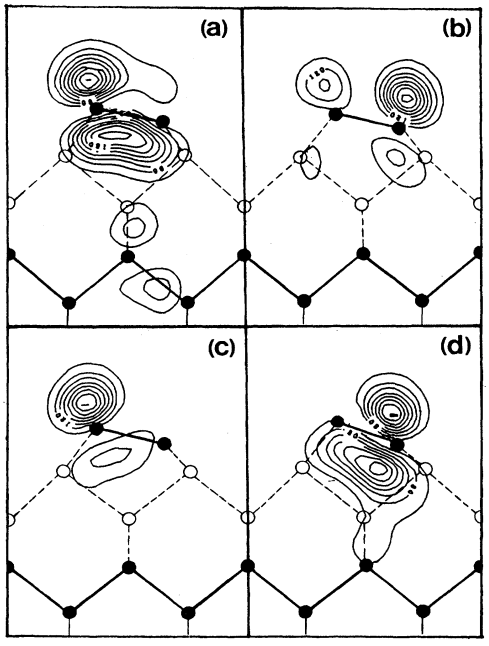

FIG. 8. Contour plots of the square of wave functions at point A in $c(4\times2)$ BZ. (a),(b) Surface bonding and antibonding states of the (2×1) system. (c),(d) Surface bonding and antibonding states of the $c(4\times2)$ system. The plotting plane and notation are the same as in Fig. 4.

The reason for this large mixing between π and π^* states at the $c(4\times2)$ case is explained as follows. By changing the symmetry of (2×1) to $c(4\times2)$, the π^* state at J' comes to interact with the π state at J [point J' in the (2×1) BZ comes to overlap with point J in the $c(4\times2)$ BZ, see Fig. 10]. As shown in Fig. 9, there emerges the matrix element between the two states, $\langle\pi^*(J')|H_{c(4\times2)}|\pi(J)\rangle$, whereas the corresponding matrix elements $\langle\pi^*(J')|H_{(2\times1)}|\pi(J)\rangle$ and $\langle\pi^*(J')|H_{p(2\times2)}|\pi(J)\rangle$ vanish because of the symmetry.

Folding the Fermi surface of the (2×1) system into the $c(4\times2)$ BZ shown in Fig. 10(c), it can also be seen that strong electron-hole interaction may appear around the region $J-Y$ of the BZ boundary when the system changes from the (2×1) symmetry into the $c(4\times2)$ one. Both properties of wave functions and Fermi surface are quite different from the $p(2\times2)$ case where the mixing and interaction are rather weak.

The above characters of electronic interactions lead to

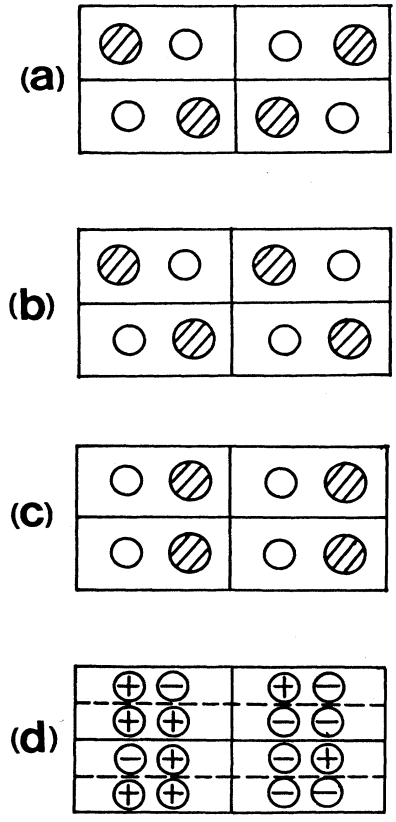

FIG. 9. Schematic illustrations of (a)–(c), the electronic potential distribution on the surfaces of $c(4\times2)$, $p(2\times2)$, and asymmetric (2×1), respectively. Larger circles represent more attractive regions; (d) phase of the wave functions. Circles above the dashed line in every (2×1) surface region represent the phase of the wave function of surface antibonding state π^* at point J'; similarly, circles below the dashed line represent that of surface bonding state π at point J.

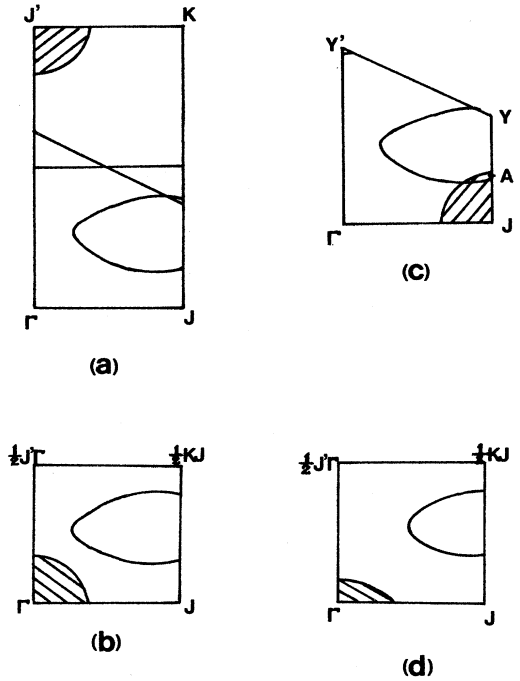

FIG. 10. Fermi surfaces of (2×1), $p(2\times2)$, and $c(4\times2)$ systems. (a) Calculated one for (2×1); (b) folded from (2×1) for $p(2\times2)$ symmetry; (c) folded from (2×1) for $c(4\times2)$ symmetry; (d) calculated one for the $p(2\times2)$ system.

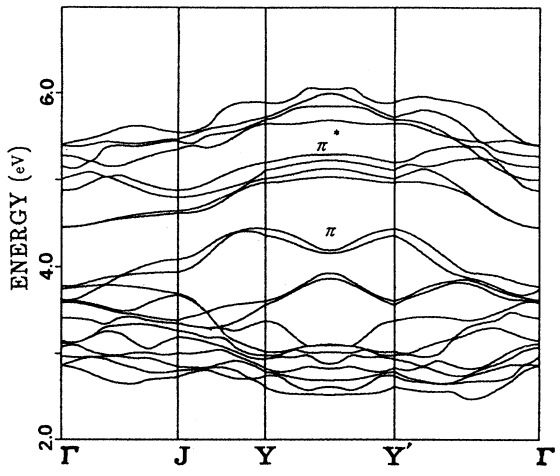

FIG. 11. Band structure of the geometry-optimized $c(4\times2)$ surface.

the surface bonding π and antibonding π^* bands at the (2×1) symmetry to be pushed away from each other for the case of the real $c(4\times2)$ system, and to open a small band gap (then the Fermi surface disappears). As seen from Fig. 7, the overlapping surface bands around the Fermi level in the folded bands [Fig. 7(b)] are separated from each other for the real case [Fig. 7(a)].

Some detailed differences of band structures among (2×1), $p(2\times2)$, and $c(4\times2)$ structures are seen from the above calculations. For example, the whole bandwidth of the occupied surface band is decreased to 0.9 eV for the $c(4\times2)$ system, and to 1.0 eV for the $p(2\times2)$ system, compared with the 1.15 eV for the asymmetric (2×1) system. The decrease of bandwidth is mainly due to the increase of distance between the nearest up-buckled atoms of the surface dimers, and therefore the weakening of interactions between them.

C. Band structures of geometry-optimized surfaces

The band structure of the geometry-optimized $c(4\times2)$ surface is given in Fig. 11 (optimized geometry of this surface will be presented in Sec. V). It shows that this surface is semiconducting with a very small indirect band gap ($\sim$0.01 eV). The lowest unoccupied band minimum is at the Γ point, which is different from the case of using the unoptimized $c(4\times2)$ geometry. The highest occupied band maximum is not largely shifted compared with Fig. 7(a); however, the whole π and π^* surface band dispersions are greatly modified. These results suggest that the surface band dispersion would be significantly changed when the surface reconstruction has a transition from the $c(4\times2)$ structure at low temperature to the (2×1) one at higher temperature. Therefore, it seems to be very interesting for the experiments to be performed on the pure $c(4\times2)$ reconstructed surface at low temperature.

For the band structure of the geometry-optimized asymmetric (2×1) surface, it is substantially the same as that in Fig. 3, and we will not present it here again. For the $p(2\times2)$ system, we have not optimized its geometry. Therefore, the real band structure of this surface is not clear. However, we expect that the real surface band structure of this reconstruction could not be substantially different from that presented here, because of the weak mixing and interaction between π and π^* surface states when symmetry changes from (2×1) to $p(2\times2)$ (see the analysis given in Sec. III B).

It is necessary to point out that the thickness of the slab (10 layers) used in this calculation is relatively thin. Interactions between two surfaces of the slab are not small enough to be ignored, and therefore the splittings between bands associated to two surfaces of the slab are large as seen from the band structures shown here. However, the features of their electronic structures are essentially reasonable and cannot be substantially changed when the thickness of the slab is increased, as we have seen in the case of the (2×1) system, presented in Sec. III A (see Fig. 5).

D. Comparison with experiments

Comparisons between experimentally observed occupied surface bands and the theoretical ones are given in Figs. 12(a)–12(c). Two experimental results are plotted in the figure, both with the angle-resolved ultraviolet

photoelectron spectroscopy (ARUPS) method.[32,33] A recent experiment on a single-domain surface by Kono's group[33] is compared to our work in Fig. 12. The experimental data have been shifted upward in energy by 0.5 eV to give the best overall agreement with the calculations. Qualitatively, the agreement between the observed and calculated bands is rather good. However, for the single-domain experiment, there appear two additional high-intensity branches, one along Γ to J, another along Y' to J', as shown in Fig. 12(a) by open circles, which cannot be theoretically explained for the ideal (2×1) surface. Moreover, the calculated bandwidth of the occupied surface band is 1.15 eV, which is larger than the experimentally observed ones (0.65 eV from Ref. 32 and 0.80 eV from Ref. 33). Also, two small peaks along J–K and Γ–J' in the calculated dispersion are not observed by the experiments. One possible explanation for these differences is the presence of $c(4\times2)$ and $p(2\times2)$ reconstructions on the experimentally used surface.

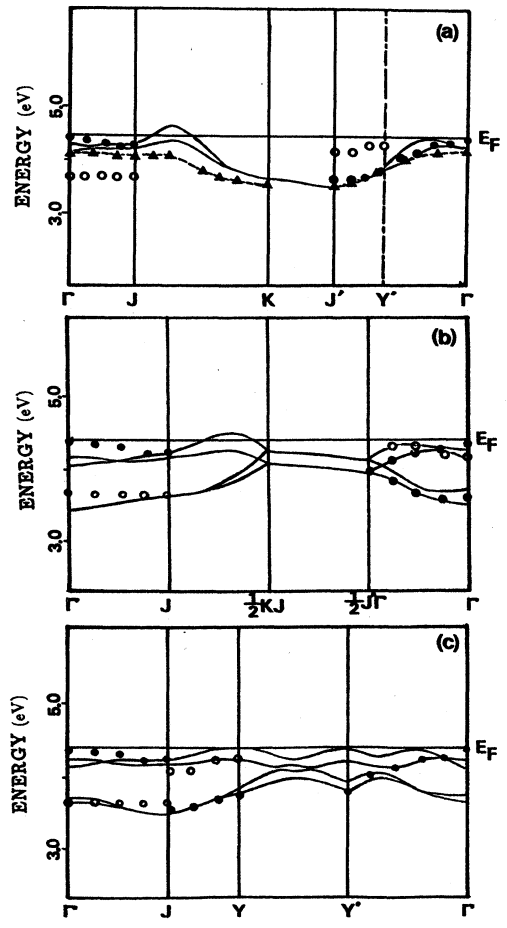

FIG. 12. Comparison of energy dispersions with ARUPS experiments (a) in a (2×1) BZ, (b) in a $p(2\times2)$ BZ, and (c) in a $c(4\times2)$ BZ. Solid triangles represent experimental data from Ref. 32. Solid and open circles represent the data from Ref. 33.

As shown in Figs. 12(b) and 12(c), where we have replotted the experimental data of Ref. 33 in $p(2\times2)$ and $c(4\times2)$ BZ together with the theoretically calculated band dispersions, both the two additional branches in Fig. 12(a) which cannot be explained by single-domain (2×1) BZ have here their corresponding branches of surface bands. Therefore, the coexistence of these higher reconstructions could be the reason for these additional observed branches.

As for the wider bandwidth obtained from calculation compared with experimental ones, there are several reasons. The bandwidths of the occupied surface band near the Fermi level of $p(2\times2)$ and $c(4\times2)$ surfaces are both decreased compared with that of the (2×1) surface, with values of 0.15 and 0.25 eV, respectively. Therefore, the influence of additional domains of higher-order reconstructions will lead to a smaller bandwidth detected in the experiments. Also, results from experiments show different values of this bandwidth. Two experiments shown here have results of 0.65 eV (Ref. 32) and 0.80 eV,[33] respectively. Another factor in accounting for the wider theoretical bandwidth is the thickness of the slab used in the calculation. It leads to a 10% decrease ($\sim$0.1 eV) of this bandwidth when a slab with 12 silicon layers is used in the calculation of the (2×1) system.

Further detailed comparison between the energy dispersions from theory and experiments would be difficult. However, considering that the existence of $p(2\times2)$ and $c(4\times2)$ domains on the (2×1) surface will make two peaks along J–K and Γ–J' lines of the (2×1) dispersion even weaker, the fact that they have not been observed by the experiments is reasonable.

IV. TOTAL ENERGIES AND GROUND STATE OF Si(100)2×1, $p(2\times2)$, AND $c(4\times2)$ STRUCTURES

The differences of energy components among (2×1), $p(2\times2)$, and $c(4\times2)$ systems are presented in Table III. The main results of their energy difference are as follows: the $c(4\times2)$ system has the lowest total energy, 0.023 eV/dimer lower than that of the asymmetric (2×1) system, and 0.011 eV/dimer lower than that of the $p(2\times2)$ one. The $p(2\times2)$ system also has lower energy than the asymmetric (2×1) system by 0.013 eV/dimer.

The total energy can be decomposed as

$$E_{\rm tot}=E_{\rm kin}+E_{e\text{-}c}+E_{e\text{-}e}+E_{\rm xc}+E_{c\text{-}c}\ . \tag{4.1}$$

The individual components can be interpreted as the electronic kinetic energy ($E_{\rm kin}$), the electron-core interaction energy $E_{e\text{-}c}$, the electron-electron Coulomb energy $E_{e\text{-}e}$, the electronic exchange and correlation energy $E_{\rm xc}$, and the core-core Coulomb energy $E_{c\text{-}c}$, respectively. As seen from Table III, the lowered total energy of the $p(2\times2)$ structure compared with the (2×1) structure is due to the decrease in core-core Coulomb energy $E_{c\text{-}c}$ and electron-electron Coulomb energy $E_{e\text{-}e}$, and also in exchange-correlation energy $E_{\rm xc}$. The decrease in $E_{c\text{-}c}$ and $E_{e\text{-}e}$ can be understood from their different atomic configurations of $p(2\times2)$ and (2×1) on the surface, that is, the distance between up-buckled atoms or down-

TABLE III. Differences of energies among asymmetric (2×1), $p(2\times2)$, and $c(4\times2)$ systems. Their geometries have the same subsurface atomic positions as shown in Fig. 2.

Energy component (eV/dimer)	$E_{p(2\times2)}-E_{(2\times1)}$	$E_{c(4\times2)}-E_{(2\times1)}$	$E_{c(4\times2)}-E_{p(2\times2)}$
$E'_{c\text{-}c}$	−0.616	0.204	0.820
$E'_{e\text{-}e}$	−0.933	0.398	1.331
$E'_{e\text{-}c}$	1.545	−0.671	−2.216
E_{kin}	0.013	0.064	0.051
Exchange	−0.022	−0.018	0.003
Total energy	−0.013	−0.023	−0.011

buckled atoms in the $p(2\times2)$ system is largely increased compared with the (2×1) case. As for the energy-increase parts, they are the kinetic energy and electron-core interaction energy. These energy increases are mainly due to the charge increase around the up-buckled dimer atoms in the $p(2\times2)$ case. As shown in Fig. 13, which is the contour plot for the total charge density differences between $p(2\times2)$ and (2×1) systems at the dimer with the same buckling direction, the electronic charge density around the up-buckled dimer atom is increased in the $p(2\times2)$ system.

As for the energy lowering for the $c(4\times2)$ surface compared with the (2×1) surface, the decreased energy components are the electron-core interaction energy $E_{e\text{-}c}$ and the exchange-correlation part E_{xc}. In contrast with the case of the $p(2\times2)$ surface, the core-core Coulomb energy $E_{c\text{-}c}$ and the electron-electron Coulomb energy $E_{e\text{-}e}$ are increased. The charge difference between $c(4\times2)$ and (2×1) systems shows the same character as that of $p(2\times2)$ and (2×1) systems, similar to Fig. 13, but with a slightly larger increase of electronic charge around the up-buckled dimer-atoms, and a decrease around the down-buckled dimer atoms, compared to the $p(2\times2)$ case. The differences of the above energy parts are similarly due to the different atomic configurations on the surface together with the different ionic degree of the surface dimer atoms.

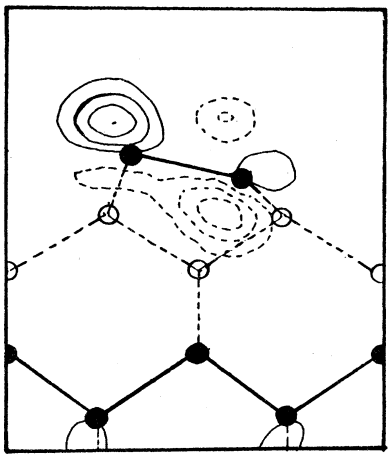

FIG. 13. Contour plot of the total charge difference between $p(2\times2)$ and asymmetric (2×1) systems. Solid and dashed lines represent increase and decrease regions, respectively. The plotting plane and notation are the same as in Fig. 4.

The comparison of energies between $c(4\times2)$ and $p(2\times2)$ systems can be helpful in understanding the ground state of the Si(100) surface. It shows that energy components are decreased only in the electron-core interaction part and all other energy components are increased. The reason for the above result can be understood as follows: the significant π and π^* mixing as explained in Sec. III B, which occurs only in the $c(4\times2)$ case, will cause the electronic charge to accumulate around the up-buckled dimer atoms, as shown in Fig. 8(c). These charges feel a deeper potential of the core of the on-site and also intersite up-buckled dimer atoms, compared with the case of $p(2\times2)$. This effect contributes to the lowering of the electron-core energy $E_{e\text{-}c}$ as shown in Table II. It also leads to the lowering of total energy in the $c(4\times2)$ system, because it overwhelms the summation of all the increased energy components, that is, the Coulomb repulsive energy, kinetic energy, and exchange-correlation energy.

Since geometries used for the above systems are not the energy-minimum ones, the atoms in the unit cell are constrained for $p(2\times2)$ and $c(4\times2)$ systems. The energy difference presented here only shows that the ordering of surface dimers with $c(4\times2)$ symmetry can be relatively more stable than that with $p(2\times2)$ symmetry. It provides evidence for supporting the $c(4\times2)$ structure as the ground state of this surface.

Larger energy differences are expected between the above systems after the optimization of their geometries. We have optimized the geometries of $c(4\times2)$ and asymmetric (2×1) systems, which will be presented in the next section. The difference of total energy between geometry-optimized $c(4\times2)$ and (2×1) becomes −0.067 eV/dimer.

V. OPTIMIZED GEOMETRIES OF ASYMMETRIC (2×1) AND $c(4\times2)$ SYSTEMS

The optimized geometries of asymmetric (2×1) and $c(4\times2)$ structures are given in Tables IV and V together

TABLE IV. The atomic displacements (units of Å) of the asymmetric (2×1) surface obtained by theoretical calculations and experiment (Ref. 35). YC refers to the result of Yin and Cohen (Ref. 16). The coordinates for the ideal surface are given by the indices (k,l,m), $R=(k\times a/2\times\sqrt{2}, l\times a/2\times\sqrt{2}, m\times a/4)$, in which a is the lattice constant of bulk silicon, and the coordinate frame is defined in Fig. 14.

Atoms		Expt.			Present calc.			YC	
(k,l,m)	Δx	Δy	Δz	Δx	Δy	Δz	Δx	Δy	Δz
(0,0,0)	0.500	0.0	−0.250	0.591	0.0	−0.106	0.573	0.0	−0.159
(2,0,0)	−0.900	0.0	−0.614	−1.045	0.0	−0.471	−1.038	0.0	−0.468
(0,1,−1)	0.094	0.0	−0.022	0.115	0.0	0.012	0.093	0.0	−0.047
(2,1,−1)	−0.105	0.0	0.055	−0.140	0.0	0.021	−0.115	0.0	0.020
(1,1,−2)	−0.016	0.0	−0.146	−0.059	0.0	−0.196	−0.007	0.0	−0.185
(3,1,−2)	−0.002	0.0	0.131	−0.005	0.0	0.177	−0.034	0.0	0.129
(1,2,−3)	0.026	0.0	−0.112	0.006	0.0	−0.155	0.061	0.0	−0.135
(3,2,−3)	−0.032	0.0	0.100	−0.007	0.0	0.136	−0.060	0.0	0.103
(0,0,−4)				−0.078	0.0	0.007			
(2,0,−4)				0.085	0.0	−0.012			

with those determined by experiments or other calculation. The important difference for optimizing the geometries of (2×1) and $c(4\times2)$ structures is the atomic relaxation freedoms. For the $c(4\times2)$ system, atoms can relax along all directions; however, relaxations for the (2×1) system are confined only in the x-z plane [the coordinate frame is defined in Fig. 14 for both the (2×1) and $c(4\times2)$ systems]. This difference also contributes to the relative stability of the $c(4\times2)$ structure at low temperature.

From the coordinates given in Table IV for the asymmetric (2×1) structure, we can compute the bond lengths between the atoms. The dimer bond length in this calculation (2.22 Å) is shorter than the bulk single-bond length (2.35 Å) and longer than the double-bond length (2.14 Å), as similar to Yin and Cohen's (YC) results (2.25 Å),[16] but the tilting angle of surface dimer at the present calculation (9.5°) is larger compared with that calculated by Yin and Cohen (8°). The backbond length between atoms 1-5 (see Fig. 14) is 2.33 Å, nearly the same as the bulk one. Another backbond length between atoms 2 and 6 is 2.29 Å, compressed by a small amount (2.5%). The remaining bonds in the system are changed less than 2% of the bulk values. Since many geometries for the (2×1) surface have been presented by experiments, we select the recent one. In this analysis,[37]

TABLE V. The atomic displacements (units of Å) of the $c(4\times2)$ surface obtained by the present calculation and experiment (Ref. 36). The coordinate frame and other notations are the same as in Table IV.

	Atoms		Expt.			Present calc.	
	(k,l,m)	Δx	Δy	Δz	Δx	Δy	Δz
Layer 1	(0,0,0)	0.593	0.000	0.170	0.667	0.012	−0.034
	(2,0,0)	−0.954	0.000	−0.460	−0.957	0.010	−0.577
	(6,0,0)	−0.593	0.000	0.170	−0.667	−0.012	−0.034
	(4,0,0)	0.954	0.000	−0.460	0.957	−0.010	−0.577
Layer 2	(0,1,−1)	0.092	−0.113	0.071	0.122	−0.077	−0.030
	(2,1,−1)	−0.092	0.113	0.071	−0.122	0.077	−0.030
	(4,1,−1)	0.092	0.113	0.071	0.139	0.091	−0.020
	(6,1,−1)	−0.092	−0.113	0.071	−0.139	−0.091	−0.020
Layer 3	(1,1,−2)	0.000	0.000	−0.057	0.000	0.000	−0.241
	(3,1,−2)	0.000	0.004	0.166	0.021	0.005	0.153
	(5,1,−2)	0.000	0.000	−0.057	0.000	0.000	−0.241
	(7,1,−2)	0.000	−0.004	0.166	−0.021	−0.005	0.153
Layer 4	(−1,2,−3)	0.000	0.000	0.137	0.000	0.000	0.123
	(1,2,−3)	−0.033	0.000	−0.029	−0.012	0.005	−0.193
	(3,2,−3)	0.000	0.000	0.127	0.000	0.000	0.123
	(5,2,−3)	0.033	0.000	−0.029	0.012	−0.005	−0.193
Layer 5	(0,2,−4)	−0.056	0.000	0.035	−0.096	−0.002	−0.014
	(2,2,−4)	0.027	0.000	0.056	0.082	0.010	−0.008
	(4,2,−4)	−0.027	0.000	0.056	−0.082	−0.010	−0.008
	(6,2,−4)	0.056	0.000	0.035	0.096	0.002	−0.014

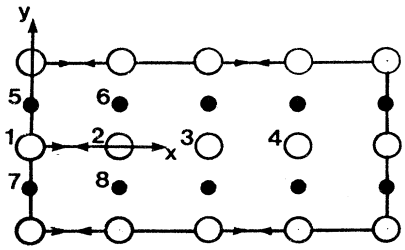

FIG. 14. Coordinate frame defined for (2×1) and $c(4\times2)$ systems.

the bond length of the surface dimer is 2.47 Å, longer than that of the bulk bond. The tilting angle of the dimer is 8.5°, a little smaller than that of the present calculation (9.5°). Bond lengths of two backbonds of atoms 1-5 and 2-6 are 2.26 and 2.18 Å, both more compressed compared with our calculation.

For the optimized geometry of the $c(4\times2)$ system, some features of atomic relaxations along the y direction have been seen. For example, there is a very small shift of the surface dimers along the y direction that is not yet detected by experiments. Also, present theoretical calculation reveals that the up-buckled surface dimer atom pulls two neighboring atoms of the second surface layer inward, and accordingly, the down buckling of the surface dimer atom pushes two neighboring second-layer atoms outward. These features are similar to those obtained by *ab initio* molecular-dynamics calculation on the Ge(100) $c(4\times2)$ surface.[38] There is a common feature in the atomic relaxation for the dimerized surface, that is, the top-layer atomic dimer will cause the second-layer atoms to move close to each other in the same direction as the dimerization, although in a largely reduced magnitude. These features of distortion are in good agreement with the experiments.

From our calculation, the surface dimer bond length of $c(4\times2)$ is 2.27 Å, which is a little longer than that of the (2×1) case (2.22 Å) but still shorter (3.4%) than the bulk one. The tilting angle of the surface dimer is 14°, which is larger than that of the asymmetric (2×1) system (8.5°), showing larger dimer buckling. The backbonds of atoms 1-5, 1-7, 2-6, and 2-8 are 2.34, 2.33, 2.30, and 2.33 Å, respectively, and all are near the bulk value. In the experiment,[39] the bond length of the surface dimer is 2.37 Å, nearly the same as the bulk value. Backbonds of surface dimers are also all around 2.37 Å. These values are a little longer than the calculated ones. The tilting angle of the surface dimer is 15.5° from this experiment, in good agreement with the theoretical prediction. For deeper layers, the directions of atomic distortions and the orders of distortions are all in good agreement with experiment and present calculation. Generally speaking, the agreement between experiment and present calculation for the $c(4\times2)$ geometry is reasonably good.

VI. SUMMARY

In this paper, we have presented theoretical studies of electronic and geometric structure of several reconstructed surfaces of silicon (100), i.e., (2×1) surfaces with symmetric and asymmetric dimers, $p(2\times2)$, and $c(4\times2)$ reconstructions, by using the self-consistent norm-conserving nonlocal pseudopotential method with a repeated slab model. Our study concentrated on the dimer model which is now most widely accepted. Main results of present work are summarized as follows. (a) Symmetric dimer model of (2×1) surface results in metallic surface bands. Total energy of this model is 0.25 eV/dimer higher than that of asymmetric model. This is consistent with past theoretical calculations. (b) An energy-minimized geometry of the asymmetric (2×1) system is presented, which has 0.14 eV/dimer energy lower than available theoretically optimized geometry by using the local pseudopotential method.[16] Atomic distortions up to five surface layers are given for the new geometry. (c) Although the buckling of dimer atoms pushes two surface bands remarkably away from each other, the surface bands of the asymmetric dimer model of the (2×1) surface still remain metallic. (d) Surface electronic structures of $p(2\times2)$ and $c(4\times2)$ systems are presented. The electronic feature of the $p(2\times2)$ surface is also metallic like that of asymmetric (2×1) surface, however, that of the $c(4\times2)$ surface is semiconducting. These results are analyzed and understood based on the electronic feature of the (2×1) asymmetric dimer surface. (e) The surface band dispersions are compared with ARUPS experiments. It shows reasonably good agreement. (f) We have calculated the total energies of (2×1), $p(2\times2)$, and $c(4\times2)$ systems with the exact same subsurface relaxations and same buckling amount of a single dimer. Results show that the $c(4\times2)$ system has the lowest total energy with 0.011 eV/dimer energy lower than that of the $p(2\times2)$ system, and 0.023 eV/dimer lower than the (2×1) system. Therefore, by the present calculation, the $c(4\times2)$ system can be the most favorable one in energy at low temperature. (g) Optimized geometry for the $c(4\times2)$ system is presented, in generally good agreement with experiment.[37] The energy difference between the $c(4\times2)$ and asymmetric (2×1) systems becomes -0.067 eV/dimer after the optimization of their geometries and the conduction-band minimum of the $c(4\times2)$ surface comes to Γ point with a very small indirect band gap.

ACKNOWLEDGMENTS

The authors are indebted to Dr. K. Shiraishi and Dr. T. Ohno for providing us with the calculational programs and pseudopotential of silicon, and to Professor M. Nakayama for valuable discussions. We would also like to thank Professor S. Kono for providing us with new experimental data prior to publication. One of the authors (Z.Z.) would also like to thank Dr. S. Ohnishi (Fundamental Research Laboratories, NEC Corporation) and many other Japanese colleagues for making his staying in Japan possible. Numerical calculations were performed on the Hitachi HITAC-S820 at the Computer Center of the University of Tokyo, and at the Computer Center of the Institute for Molecular Science. This work was supported in part by a Grant-in-Aid from the Ministry of Education, Science and Culture, Japan.

*On leave from Department of Physics, Fudan University, Shanghai 200433, People's Republic of China.
[1]R. E. Schlier and H. E. Farnsworth, J. Chem. Phys. **30**, 917 (1959).
[2]F. Jona, H. D. Shih, A. Ignatiev, D. W. Jepsen, and P. M. Marcus, J. Phys. C **10**, L67 (1977).
[3]S. J. White and D. P. Woodcuff, Surf. Sci. **64**, 131 (1977).
[4]S. Y. Tong and A. L. Maldondo, Surf. Sci. **78**, 459 (1978).
[5]M. J. Cardillo and G. E. Becker, Phys. Rev. B **21**, 1497 (1980).
[6]J. Ihm, D. H. Lee, J. D. Joannopoulos, and J. J. Xiong, Phys. Rev. Lett. **51**, 1872 (1983).
[7]J. J. Lander and J. Morrison, J. Chem. Phys. **37**, 729 (1962).
[8]T. D. Poppendieck, T. C. Ngoc, and M. B. Webb, Surf. Sci. **43**, 647 (1974); **75**, 287 (1978).
[9]M. Aona, Y. Hou, C. Oshima, and Y. Ishizawa, Phys. Rev. Lett. **49**, 567 (1982).
[10]H. Wang, R. Lin, and X. Wang, Phys. Rev. B **36**, 7712 (1987).
[11]J. A. Martin, D. E. Savage, W. Moritz, and M. G. Lagally, Phys. Rev. Lett. **56**, 1936 (1986).
[12]T. Aruga and Y. Murata, Phys. Rev. B **34**, 5654 (1986).
[13]J. A. Appelbaum and D. R. Hamann, Surf. Sci. **74**, 21 (1978).
[14]D. J. Chadi, Phys. Rev. Lett. **43**, 43 (1979).
[15]J. Ihm, M. L. Cohen, and D. J. Chadi, Phys. Rev. B **21**, 4592 (1980).
[16]M. T. Yin and M. L. Cohen, Phys. Rev. B **24**, 2303 (1981).
[17]G. P. Kerker, S. G. Louie, and M. L. Cohen, Phys. Rev. B **17**, 706 (1978).
[18]W. S. Verwoerd, Surf. Sci. **103**, 404 (1981).
[19]W. S. Yang, F. Jona, and P. M. Marcus, Phys. Rev. B **28**, 2049 (1983).
[20]R. M. Tromp, R. J. Hamers, and J. E. Demuth, Phys. Rev. Lett. **55**, 1303 (1985).
[21]R. J. Hamers, R. M. Tromp, and J. E. Demuth, Phys. Rev. B **34**, 5343 (1986).
[22]R. Seiwatz, Surf. Sci. **2**, 473 (1964).
[23]D. J. Chadi, J. Vac. Sci. Technol. **16**, 1290 (1979).
[24]J. E. Northrup, Phys. Rev. Lett. **54**, 815 (1985).
[25]J. C. Phillips, Surf. Sci. **40**, 459 (1973).
[26]T.Tabata, T. Aruga, and Y. Murata, Surf. Sci. **179**, L63 (1986).
[27]M. T. Yin and M. L. Cohen, Phys. Rev. Lett. **45**, 1004 (1980); Phys. Rev. B **26**, 5668 (1982).
[28]G. B. Bachelet, D. R. Hamann, and M. Schlüter, Phys. Rev. B **26**, 4199 (1982).
[29]T. Ohno (unpublished).
[30]K. Shiraishi, and H. Kamimura, Mater. Sci. Eng. B **3**, 287 (1989).
[31]J. D. Levine, Surf. Sci. **34**, 90 (1973).
[32]R. I. G. Uhrberg, G. V. Hansson, J. M. Nicholls, and S. A. Flödstrom, Phys. Rev. B **24**, 4684 (1981).
[33]S. Kono (unpublished).
[34]P. Kruger and J. Pollmann, Phys. Rev. B **38**, 10578 (1988).
[35]K. C. Pandey (unpublished).
[36]M. S. Hybertsen and S. G. Louie, Phys. Rev. B **34**, 5390 (1986).
[37]B. W. Holland, C. B. Duke, and A. Paton, Surf. Sci. **140**, L269 (1984).
[38]M. Needels, M. C. Payne, and J. D. Joannopoulos, Phys. Rev. Lett. **58**, 1765 (1987).
[39]R. M. Tromp, R. G. Smeenk, F. W. Saris, and D. J. Chadi, Surf. Sci. **133**, 137 (1983).